energies

MDPI

Article

Control Effect of Deposition Processes on Shale Lithofacies and Reservoirs Characteristics in the Eocene Shahejie Formation (Es4s), Dongying Depression, China

Yepeng Yang [1,2], Zaixing Jiang [1,2,*], Jianguo Zhang [1,2], Zongxuan Zhang [1,2] and Chun Yang [1,2]

[1] School of Energy Resources, China University of Geosciences (Beijing), Beijing 100083, China
[2] Key Laboratory of Marine Reservoir Evolution and Hydrocarbon Enrichment Mechanism, Ministry of Education, China University of Geosciences (Beijing), Beijing 100083, China
* Correspondence: jiangzx@cugb.edu.cn

Abstract: The lacustrine fine-grained sedimentary rocks in the upper interval of the fourth member of the Eocene Shahejie Formation (Es4s) in the Dongying Depression are important shale oil exploration targets in Bohai Bay Basin. They are widely distributed and rich in organic matter. In this study, samples were observed under the optical microscope and FESEM, combined with geochemical test and physical property analysis to study the sedimentary characteristics and reservoir characteristics of them. Nine lithofacies are recognized based on the mineral composition, the content of organic matter and the beddings. The middle-high organic laminated calcareous fine-grained sedimentary rocks (LF1) and the middle-high organic laminated mixed fine-grained sedimentary rocks (LF2) resulted from seasonal sediment variations and settled by suspension in the deep lake. The middle-high organic flaggy mixed fine-grained sedimentary rocks (LF3), the middle-high organic flaggy calcareous fine-grained sedimentary rocks (LF4), the middle-high organic massive calcareous fine-grained sedimentary rocks (LF5) and the middle organic massive mixed fine-grained sedimentary rocks (LF6) were formed by redeposition. The low organic massive argillaceous fine-grained sedimentary rocks (LF7), the low organic massive felsic fine-grained sedimentary rocks (LF8) and the low organic massive mixed fine-grained sedimentary rocks (LF9) are affected by the terrigenous input events. The pore structures vary in different beddings which are influenced by the kinds and arrangement of minerals and particles. In the laminated lithofacies, the ink-bottle-shaped pores are dominant. In the flaggy and massive lithofacies, the ink-bottle-shaped pores and the slit-shaped pores coexist. LF1 and LF2 are the best target for shale oil exploration and the LF3, LF4, LF5 and LF6 are the second. The deposition processes control the lithofacies and reservoir characteristics of the fined-grained sedimentary rocks.

Keywords: Dongying Depression; Eocene Shahejie Formation; shale; lithofacies; reservoir characteristics

Citation: Yang, Y.; Jiang, Z.; Zhang, J.; Zhang, Z.; Yang, C. Control Effect of Deposition Processes on Shale Lithofacies and Reservoirs Characteristics in the Eocene Shahejie Formation (Es4s), Dongying Depression, China. *Energies* **2023**, *16*, 2200. https://doi.org/10.3390/en16052200

Academic Editor: Reza Rezaee

Received: 26 January 2023
Revised: 20 February 2023
Accepted: 21 February 2023
Published: 24 February 2023

1. Introduction

Success in shale oil and gas in the United States promoted enthusiasm for exploration and exploitation of shales [1–3]. Huge breakthroughs have been made in the theory and practice of shale oil and gas exploration and development [4–10], especially in the marine shales due to their large scale and wide distribution, such as the Wolfcamp shale in the Permian Basin [11], the Barnett shale in the Ford Worth Basin [4] and the Longmaxi shale in the Sichuan Basin [12–15]. However, as there are significant differences between the lacustrine shales and the marine ones in the geological setting of the basins [3,9,16–19], although there also exist abundant lacustrine shales in continental basins in China [20,21], there still many problems with increasing the production of the shale oil and gas in the lacustrine shales [3,22].

In the main oil fields in East China, lacustrine shales are developed widely in the Mesozoic and Cenozoic continental rift basins [20,23,24]. It is uncommon that the shale oil

and gas production varies significantly even for adjacent wells at a very close distance, since the reservoir properties change more rapidly and more dramatically both in horizontal and vertical directions. One important reason is that lake basins are much smaller than the marine ones in size, which makes them more sensitive to the sediment input, climate changes and local tectonic activities [3,25,26]. All these factors have great influence on deposition processes which in turn determines the sedimentary characteristics of lacustrine shales. Composed of fine grains smaller than 62.5 μm [6], shales can be deposited from the suspension, the hyperpycnal flow and sediment gravity flows induced by tectonic activities, slides and storms in deep water [27–29]. The resulting shales exhibit distinct sedimentary characteristics such as compositions, textures and sedimentary structures which are correlated to different depositional processes [18]. As a result, the reservoir properties of the shales are definitely different. As the lake basins are relatively small-scale, when several depositional processes contribute the deposition of the fine grains, shales are more likely to present greater heterogeneity, which increases the difficulty of exploration and development of shale oil and gas [19,30].

According to previous studies, in the upper interval of the fourth member in the Eocene Shahejie Formation (Es4s) in the Dongying Depression in the Bohai Bay Basin, shales distribute widely, 250–350 m thick [31]. A large number of works have shown that these shales were deposited in the salinized deep lake environment [9,31–34] during a warm and humid period when algae were blooming [9]. As a result, these shales are thick-bedded and organic-rich reservoirs with great potential for shale oil and gas exploration [29,31], and appropriate objects to study the depositional processes of organic-rich shales. Many researches of these shales reported that they could be classified into laminated lithofacies and massive lithofacies [29,35–37]. The laminated ones were interpreted to be deposited in quiet and low-energy water while the massive ones were considered to be related to rapidly deposited sorts [29,38]. However, in our work, some massive dolomites were found as interlayers in these shales which cannot be interpreted via the rapid deposition. On the other hand, numerous works have been performed to study how the diagenesis and interaction of hydrocarbons affected the pore structures [39,40]. There are also a lot of studies that focused on quantitatively evaluating the reservoir properties such as pore types, pore volume and pore size distribution of these shales [36,39–42]. All these factors are influenced by the micro-structures which are determined by the deposition processes. However, since most of the studies on deposition and reservoir properties are isolated, much uncertainty still exists between the deposition processes and reservoir properties.

In this study, we analyzed and presented the mineral composition, sedimentary structures and organic matter origin of fine-grained sedimentary rocks in Es4s in the Dongying Depression. We discussed the sedimentary characteristics and the formation mechanisms of each lithofacies. Then we characterized reservoir qualities of the different lithofacies. In accordance with the analysis above, we identified the relationship between the pore structures and the sedimentary structures, and studied the control effect of deposition processes on lithofacies and reservoir characteristics of shales in the study area. Finally, we summarized the favorable lithofacies for shale oil and gas exploration. We hope this can be helpful for promoting understanding and exploitation of the lacustrine shale oil and gas.

2. Geological Setting

The Dongying Depression is located in the southeastern corner of the Bohai Bay Basin and trends NEE (Figure 1a,c) [43]. Controlled by faults in the north margin, it is a typical half-graben basin. The Dongying Depression is bordered by the Linfanjia Uplift and Qingcheng Uplift to the west, the Qingtuozi Uplift to the northeast, the Binxian Uplift and Chenjiazhuang Uplift to the north and the Luxi Uplift and the Guangrao Uplift to the south (Figure 1c), which cover an area of 5700 km^2 [44]. It is divided into four sags by secondary fault, including Lijin Sag, Boxing Sag, Niuzhuang Sag and Minfeng Sag.

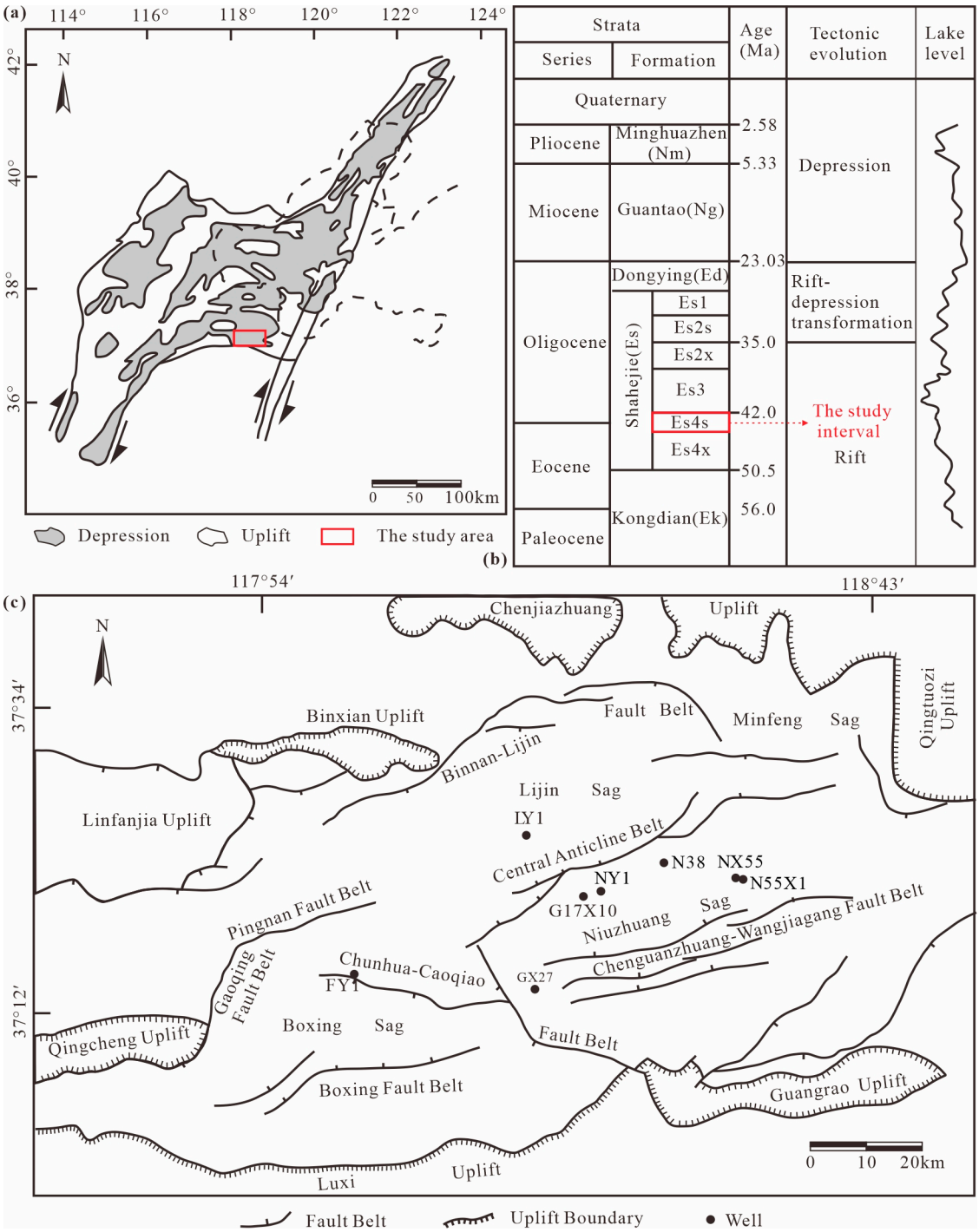

Figure 1. (**a**) The structural map of Bohai Bay Basin and the location of Dongying Depression (modified after [29]). (**b**) The strata and tectonic evolution of the Dongying Depression (modified after [45]). (**c**) The structural map of the Dongying Depression showing key well locations (used with permission and modified from the Geoscience Research Institute of Shengli Oilfield Company).

The Dongying Depression is filled by Cenozoic strata (Figure 1b), including the Kongdian (Ek), Shahejie (Es), Dongying (Ed), Guantao (Ng), Minghuazhen (Nm) and Pingyuan (Qp) Formations from bottom to top [46]. The Shahejie Formation (Es) in the Eocene is divided into four members, which are Es4, Es3, Es2 and Es1, from bottom to top. The fourth member of the Shahejie Formation (Es4) is subdivided into the Upper Es4 Interval (Es4s) and the Lower Es4 Interval (Es4x) (Figure 1b). The shales in Es4s were

deposited in the deep lake when the depression intensely rifted, accompanied with lake basin expanding rapidly and water level rising [15]

3. Materials and Methods

Data and samples for this research regard 8 wells in the Dongying Depression. We observed well cores and thin sections. Some samples were observed through field emission scanning electron microscope (FESEM). The X-ray diffraction data, the total organic carbon (TOC) content nuclear magnetic resonance data and nitrogen adsorption data were provided by the Geoscience Research Institute of Shengli Oilfield Company, SINOPEC, Dongying City, Shandong Province.

The thin section observation was completed at China University of Geosciences, Beijing. Thin sections at a thickness of 0.03 mm were observed under a polarized optical Zeiss microscope (Axio Scope A1) to identify mineral characteristics and microstructures. The microscope was manufactured by Carl Zeiss in Jena, Germany.

FESEM samples were polished via Ar ion-beam milling and observed via a Zeiss Supra 55 Sapphire field emission scanning electron microscope equipped with Genesis 2000 X-ray energy dispersive spectroscopy (EDS) after Pt coating, under an accelerating voltage of 10 kV and a working distance of 15 mm. The FESEM was manufactured by Carl Zeiss in Jena, Germany. This was completed at China University of Geosciences, Beijing.

4. Results

4.1. Mineral Composition

The fine-grained sedimentary rocks in the Es4s in Dongying Depression are composed of carbonate minerals, clay minerals, quartz, feldspar, pyrite and a small amount of other minerals (Table 1). Based on the XRD analysis, carbonate minerals (average: 50.85 wt%) are the dominant minerals which include the calcite (average: 37.20 wt%) and the dolomite (average: 13.65 wt%). The content of calcite ranges from 0 to 85 wt% and the content of dolomite ranges from 0 to 79 wt%. The content of clay minerals ranges from 4 to 52 wt% with an average of 21.18 wt% and include illite (average: 74.17 wt%), illite/smectite mixed layers (average: 22.39 wt%), kaolinite (average: 1.89 wt%) and chlorite (average: 1.55 wt%). The content of the quartz varies from 6 to 41 wt% and the average content is 18.33 wt%. The content of feldspar is from 0 to 22 wt%, with an average of 4.64 wt%. The grain size of quartz and feldspar is mainly clay- to silt-size. The average content of pyrite is 3.12 wt%. The pyrites mainly exist as framboids and a small number of individual crystals.

4.2. Lithofacies

To summarize more sedimentary characteristics of fine-grained sedimentary rocks, the lithofacies classification considers three main parts: mineral composition, bedding and the content of TOC [18,47]. Based on the ternary compositional diagram of the relative content of the carbonate minerals, clay minerals and felsic minerals, the fine-grained sedimentary rocks can be divided into the argillaceous, calcareous, felsic and mixed ones (Figure 2) [18]. We recorded the variations in beddings at the centimeter scale in cores and divided them into the following three types according to the thickness of one bedding: laminated (less than 1 cm), flaggy (1–5 cm) and massive (more than 5 cm) in this study [24,48]. According to the content of TOC, the fine-grained sedimentary rocks are divided into the low organic (TOC < 2 wt%), middle organic (2 wt% < TOC < 4 wt%) and high organic (TOC > 4 wt%) ones [47]. Combined with these three factors, the fine-grained sedimentary rocks in Es4s in Dongying Depression can be divided into the following nine lithofacies: middle-high organic laminated calcareous fine-grained sedimentary rocks (LF1), middle-high organic laminated mixed fine-grained sedimentary rocks (LF2), middle-high organic flaggy mixed fine-grained sedimentary rocks (LF3), middle-high organic flaggy calcareous fine-grained sedimentary rocks (LF4), middle-high organic massive calcareous fine-grained sedimentary rocks (LF5), middle organic massive mixed fine-grained sedimentary rocks (LF6), low organic massive argillaceous fine-grained sedimentary rocks (LF7), low organic massive

felsic fine-grained sedimentary rocks (LF8) and low organic massive mixed fine-grained sedimentary rocks (LF9). The characteristics of each lithofacies are described below.

Table 1. Mineral content (wt%) of different lithofacies in the Es4s Dongying Depression.

Lithofacies		Clay Minerals	Quartz	Feldspar	Calcite	Dolomite	Pyrite	Anhydrite	Siderite	Halite	Aragonite	Barite
LF1	Average	14.77	15.49	2.67	49.94	13.38	2.16	0.19	0.66	0.85	0.07	0
	Range	4–24	3–28	0–7	6–85	0–78	0–5	0–1	0–3	0–2	0–4	0
LF2	Average	28.95	22.50	5.95	25.10	10.25	4.60	0.45	1.00	1.00	1.40	0
	Range	17–37	15–41	2–15	11–47	0–28	1–10	0–1	0–2	0–1	0–13	0
LF3	Average	32.57	23.07	9.07	19.14	9.79	3.50	0.79	1.21	1.25	0	2.00
	Range	25–43	17–32	4–22	8–35	3–28	2–8	0–2	0–2	0–2	0	0
LF4	Average	14.67	12.00	3.67	29.00	36.67	2.00	0.67	0.67	1.00	0	0
	Range	11–17	7–17	3–4	11–59	4–54	1–3	0–1	0–1	0–1	0	0
LF5	Average	15.43	15.07	2.50	39.86	23.00	2.07	0.14	1.14	0.79	0	0
	Range	6–23	7–22	1–5	0–62	0–79	0–6	0–1	0–2	0–2	0	0
LF6	Average	30.13	22.88	6.25	23.88	8.38	4.75	1.25	1.88	1.00	0	0
	Range	21–39	18–26	4–11	10–38	3–21	3–10	0–4	1–4	0–1	0	0
LF7	Average	50.33	24.67	7.33	6.33	5.67	3.67	0.67	1.00	1.00	0	0
	Range	47–52	22–28	6–9	5–8	5–9	2–5	0–2	0–2	0–1	0	0
LF8	Average	16.00	32.00	20.33	15.33	11.00	2.33	1.00	1.00	1.00	0	0
	Range	13–19	29–34	19–21	13–17	6–15	2–3	1	1	1	0	0
LF9	Average	28.70	25.80	12.53	12.63	14.20	3.03	0.80	1.50	1.00	0	0
	Range	24–41	13–27	3–11	0–39	4–36	2–5	0–1	1–3	1	0	0

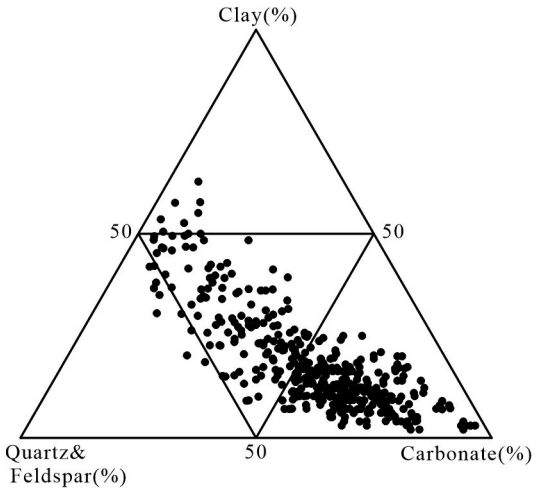

Figure 2. Ternary compositional diagram of the relative content of the carbonate minerals, clay minerals and felsic minerals of fine-grained sedimentary rocks in Es4s in Dongying Depression.

4.2.1. Middle-High Organic Laminated Calcareous Fine-Grained Sedimentary Rocks (LF1)

Middle-high organic laminated calcareous fine-grained sedimentary rocks (LF1) are grayish black or dark gray (Figure 3a). The content of TOC in them ranges from 2.00 to 9.79 wt%, with an average of 3.77 wt%. They are characterized by well developed laminae and abundant carbonate minerals (average: 63.32 wt%) (Table 1) including calcite, ferrocalcite, dolomite and ankerite (Figure 4a–c). Lamina boundaries are fairly distinct in cores and thin sections (Figures 3a and 4a–c). Laminae are continuous planar or wavy while some are curved due to deformation (Figure 4d) [18]. Under the plane-polarized light, light laminae are composed of carbonate minerals while the dark ones are mainly composed of clay minerals, organic matter, quartz and feldspar (Figure 4a–c). The light laminae and dark laminae are regularly superimposed, forming into rhythmic laminae (Figure 4a–c).

Grain size of carbonate minerals varies from 2 to 500 μm. Some sparry (grain size > 20 μm) carbonate minerals form into bedding-parallel veins whose thickness is 0.2–1.0 cm in cores and gypsum occurs in the veins (Figure 4e,f) [24]. Sinusoidal solid inclusions that are composed of quartz, feldspar, clay minerals and organic matter are developed in the veins (Figure 4e–g) [49]. On the cross section of the clay laminae, there are carbon debris locally.

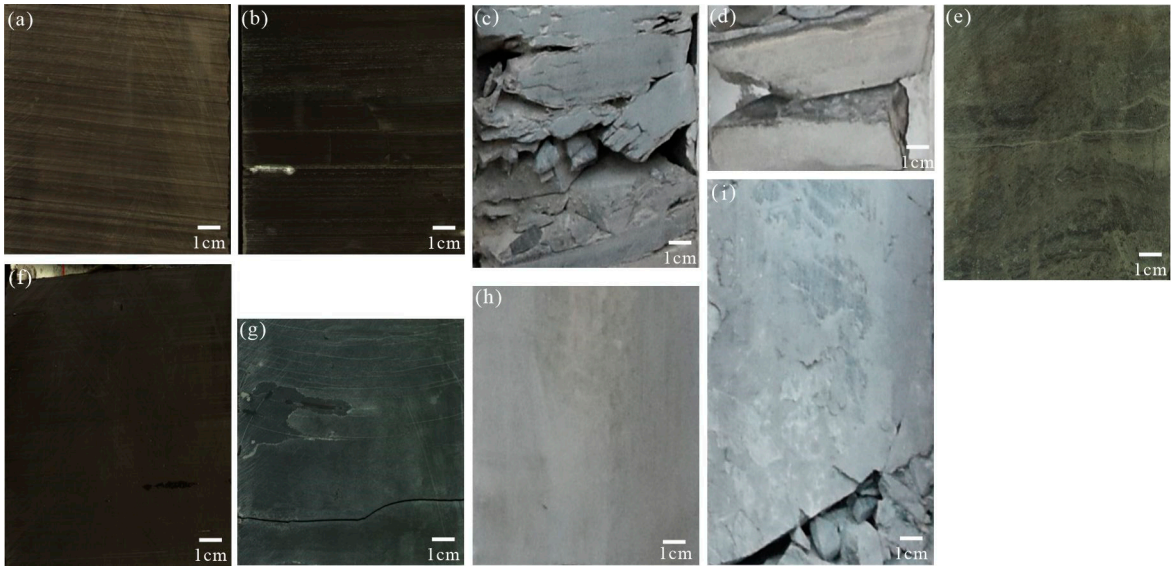

Figure 3. (**a**) Middle-high organic laminated calcareous fine-grained sedimentary rocks. Well NY1, 3419.40 m. (**b**) Middle-high organic laminated mixed fine-grained sedimentary rocks. Well NY1, 3411.20 m. (**c**) Middle-high organic flaggy mixed fine-grained sedimentary rocks. Well G17X10, 3200.15 m. (**d**) Middle-high organic flaggy calcareous fine-grained sedimentary rocks. Well G17X10, 3211.30 m. (**e**) Middle-high organic massive calcareous fine-grained sedimentary rocks. Well FY1, 3430.8 m. (**f**) Middle organic massive mixed fine-grained sedimentary rocks. Well NY1, 3449.30 m. (**g**) Low organic massive argillaceous fine-grained sedimentary rocks. Well NY1, 3471.24 m. (**h**) Low organic massive felsic fine-grained sedimentary rocks. Well G17X10, 3226.90 m. (**i**) Low organic massive mixed fine-grained sedimentary rocks. Well G17X10, 3230.05 m.

4.2.2. Middle-High Organic Laminated Mixed Fine-Grained Sedimentary Rocks (LF2)

Middle-high organic laminated mixed fine-grained sedimentary rocks (LF2) are grayish black (Figure 3b). The content of TOC in them ranges from 2.12 to 11.2 wt%, with an average of 4.64 wt%. The average content of clay minerals, quartz and feldspar and carbonate minerals are, respectively, 28.95 wt%, 28.45 wt% and 35.35 wt%. Laminae are developed but weaker than LF1 in cores and some laminae are uncontinuous. Under the plane-polarized light, carbonate minerals that exist as micritic (<5 μm) and microsparry (5–20 μm) grains form into light laminae. The dark laminae are mainly composed of clay minerals, organic matter, quartz and feldspar (Figure 4h). It is common that there are a series of fossils such as leaves, fishes and some other aquatic organisms on the cross section of the clay laminae.

4.2.3. Middle-High Organic Flaggy Mixed Fine-Grained Sedimentary Rocks (LF3)

Middle-high organic flaggy mixed fine-grained sedimentary rocks (LF3) are dark gray (Figure 3c). The content of TOC in them ranges from 2.15 to 6.01 wt% with an average of 4.06 wt%. The average content of clay minerals, quartz and feldspar and carbonate minerals are, respectively, 32.57 wt%, 32.14 wt% and 28.93 wt%. The LF3 are generally the interlayer in the LF2. They are abrupt contact with overlying and underlying laminated lithofacies in cores. Carbonate minerals mainly exist as marl mixed with clay minerals, with a small amount of sparry (>20 μm) and microsparry (5–20 μm) grains. The quartz,

feldspar, pyrite aggregates, biodetritus and carbonate grains are scattered in a disordered manner in marl and clay minerals in a flaggy bedding (Figure 4i).

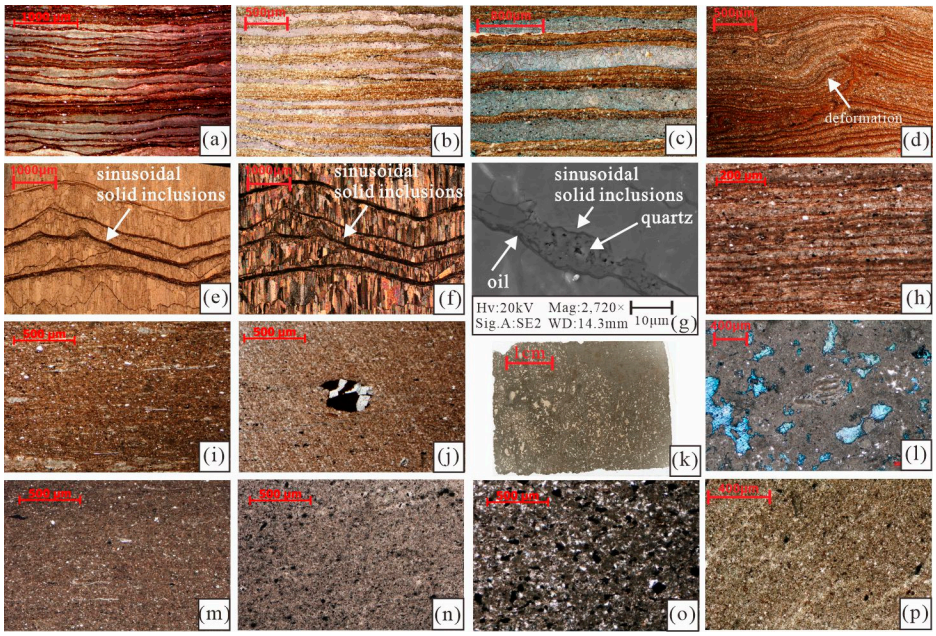

Figure 4. (**a**) The thin section of middle-high organic laminated calcareous fine-grained sedimentary rocks. Dyed calcites are red. Well NY1, 3409.77 m. (**b**) The thin section of middle-high organic laminated calcareous fine-grained sedimentary rocks. Dyed ferrocalcites are mauve. Well NX55, 3789.50 m. (**c**) The thin section of middle-high organic laminated calcareous fine-grained sedimentary rocks. Dyed ankerites are blue. Well NX55, 3784.80 m. (**d**) Laminae are curved due to deformation. Well NY1, 3341.75 m. (**e**) Sinusoidal solid inclusions that are composed of quartz, feldspar, clay minerals. The organic matter develops in the sparry ankerite veins. Well N55X1, 3588.60 m. (**f**) The photo of (**e**) under the crossed-polarized light. Gypsum occurs in the sparry ankerite lamina. Well N55X1, 3588.60 m. (**g**) Quartz, feldspar, clay minerals and organic matter in sinusoidal solid inclusions. Well N55X1, 3588.60 m. (**h**) The thin section of middle-high organic laminated mixed fine-grained sedimentary rocks. Well NY1, 3442.33 m. (**i**) The thin section of middle-high organic flaggy mixed fine-grained sedimentary rocks, Well NY1, 3339.18 m. (**j**) The thin section of middle-high organic flaggy calcareous fine-grained sedimentary rocks, Well NY1, 3360.07 m. (**k**) The scanning photo of the thin section, Well FY1, 3430.8 m. (**l**) The thin section of middle-high organic massive calcareous fine-grained sedimentary rocks. The dyed ankerite is blue. Well FY1, 3430.8 m. (**m**) The thin section of middle organic massive mixed fine-grained sedimentary rocks, Well NY1, 3362.63 m. (**n**) The thin section of low organic massive argillaceous fine-grained sedimentary rocks, Well NY1, 3471.68 m. (**o**) The thin section of low organic massive felsic fine-grained sedimentary rocks. Well NY1, 3468.65 m. (**p**) The thin section of low organic massive mixed fine-grained sedimentary rocks. Well NX55, 3789.73 m.

4.2.4. Middle-High Organic Flaggy Calcareous Fine-Grained Sedimentary Rocks (LF4)

Middle-high organic flaggy calcareous fine-grained sedimentary rocks (LF4) are gray (Figure 3d). The TOC content of them ranges from 2.77 to 4.32 wt% with an average of 3.43 wt%. Carbonate minerals are dominant components in the LF4. The average content of clay minerals, quartz and feldspar and carbonate minerals are, respectively, 14.16 wt%, 15.67 wt% and 65.67 wt%. The LF4 is generally the interlayer in the LF1 (Figure 5a). They are abrupt contact with the overlying and underlying laminated lithofacies in cores (Figure 5a). Carbonate minerals mainly exist as marl mixed with clay minerals, with a small amount of sparry (>20 μm) and microsparry (5–20 μm) grains. The quartz, feldspar, pyrite aggregates, biodetritus and carbonate grains are scattered in a disordered manner in marl and clay minerals in a flaggy bedding (Figure 4j).

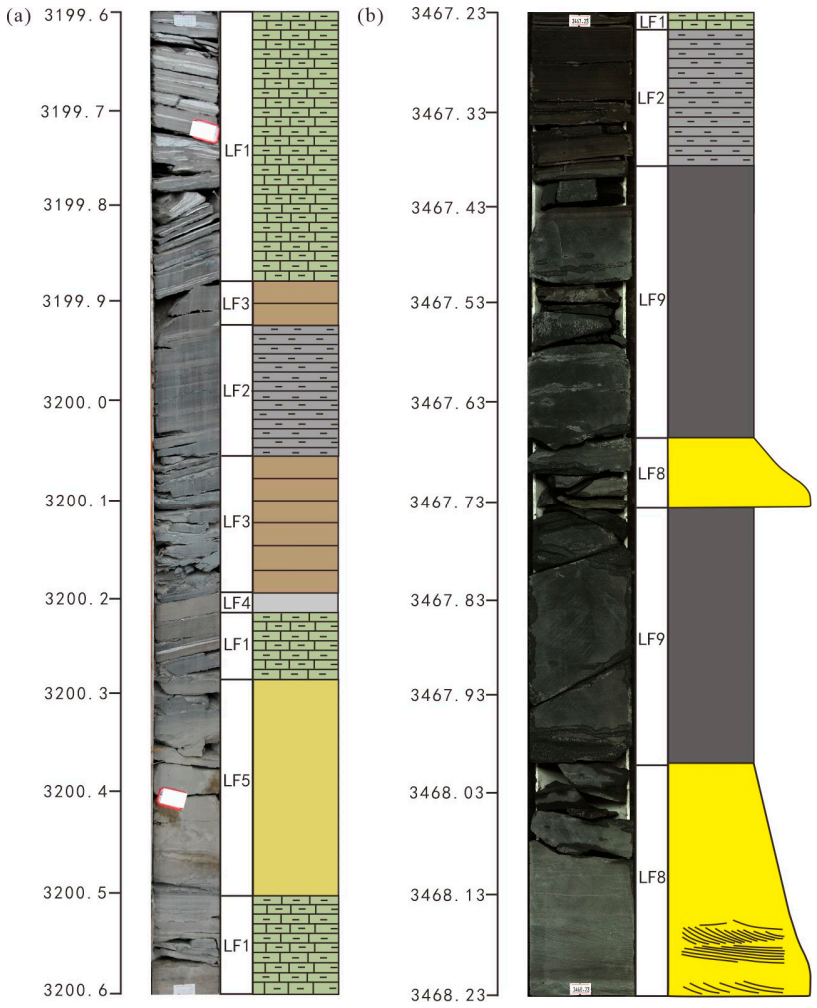

Figure 5. The lithofacies in cores. (**a**) Well NY1, 3199.6–3200.6 m; (**b**) Well NY1, 3467.23–3468.23 m.

4.2.5. Middle-High Organic Massive Calcareous Fine-Grained Sedimentary Rocks (LF5)

Middle-high organic massive calcareous fine-grained sedimentary rocks (LF5) are light gray (Figure 3e). The TOC content of them ranges from 2.02 to 8.12 wt% with an average of 3.61 wt%. The average content of clay minerals, quartz and feldspar and carbonate minerals are, respectively, 15.43 wt%, 17.57 wt% and 62.86 wt%. The content of carbonate minerals can be up to 79 wt%. Carbonate minerals also mainly exist as marl and sparry (>20 μm) grains (Figure 4k). Under the microscope, there are abundant biodetritus and some have been replaced by carbonate minerals (Figure 4k,l). The LF5 only occur locally.

4.2.6. Middle Organic Massive Mixed Fine-Grained Sedimentary Rocks (LF6)

Middle organic massive mixed fine-grained sedimentary rocks (LF6) are grayish black (Figure 3f). The TOC content of them ranges from 2.16 to 3.31 wt% with an average of 2.48 wt%. The average content of clay minerals, quartz and feldspar and carbonate minerals are, respectively, 30.13 wt%, 29.13 wt% and 32.26 wt%. Carbonate minerals also mainly exist as marl mixed with clay minerals (Figure 4m). In cores, the LF6 are continuous and up to 1 m long. They occur between the laminated lithofacies and abruptly contact with them. They are massive and homogeneous.

4.2.7. Low Organic Massive Argillaceous Fine-Grained Sedimentary Rocks (LF7)

Low organic massive argillaceous fine-grained sedimentary rocks (LF7) are grayish black (Figure 3g). The TOC content of them ranges from 0.43 to 1.29 wt% with an average of 0.68 wt%. The average content of clay minerals, quartz and feldspar and carbonate

minerals are, respectively, 50.33 wt%, 32.00 wt% and 12.00 wt%. The LF7 is charactered by high content of clay minerals which is dominated by illite and the illite/smectite mixed layers (Figure 4n). Carbonate minerals are mainly present in the form of marl. Under the microscope, the direction of the long axis of the illite and the illite/smectite mixed layers or ostracods fragments are oriented so that the cores are present indistinct horizontal beddings. Cores of the LF7 are massive and homogeneous.

4.2.8. Low Organic Massive Felsic Fine-Grained Sedimentary Rocks (LF8)

Low organic massive felsic fine-grained sedimentary rocks (LF8) are light gray (Figure 3h). The TOC content of them ranges from 0.39 to 0.64 wt% with an average of 0.48 wt%. The average content of clay minerals, quartz and feldspar and carbonate minerals are, respectively, 16.00 wt%, 50.33 wt% and 25.33 wt%. Carbonate minerals mainly exist as marl. The quartz and feldspar are dominant minerals, scattered among the clay minerals with cluttered arrangement (Figure 4o). They are generally silt-sized grains and subangular. Generally, cores of the LF8 are massive but there are wavy beddings locally (Figure 5b).

4.2.9. Low Organic Massive Mixed Fine-Grained Sedimentary Rocks (LF9)

Low organic massive mixed fine-grained sedimentary rocks (LF9) are gray (Figure 3i). The TOC content of them ranges from 0.36 to 1.62 wt% with an average of 0.95 wt%. The average content of clay minerals, quartz and feldspar and carbonate minerals are, respectively, 28.70 wt%, 38.33 wt% and 26.83 wt%. Carbonate minerals also mainly exist as marl. Quartz, feldspar and other mineral grains are scattered among the marl and clay minerals with cluttered arrangement (Figure 4p).

4.3. Organic Matter Characteristics

The plot of the hydrogen index (HI) versus the pyrolysis temperature of maximum yield of pyrolysate (T_{max}) for different lithofacies (Figure 6) reveals that the sources of organic matter in them changes from Type I to Type III. In LF1, LF2, LF3, LF4, LF5 and LF6, Type I and Type II are predominant while Type II-III and Type III-II are minority. In LF7, LF8 and LF9, the sources of organic matter are Type III-II and Type III [50,51].

4.4. Reservoir Characteristics

4.4.1. Pore Types

According to the observation, interparticle pores, intraparticle pores, lamina fissures and fractures are main pore types in the fine-grained sedimentary rocks in the Es4s in Dongying Depression [52].

1. Interparticle pores.

The intergranular pores are dominant in the study object and are developed in all nine lithofacies. In the carbonate laminae, interparticle pores are developed between carbonate crystals (Figure 7a). In the clay laminae, interparticle pores are developed between quartz, feldspar, clay minerals and pyrite aggregates (Figure 7b). Pores between clay minerals generally have a smooth edge and are oriented parallel to the lamina (Figure 7b). In flaggy and massive rocks, interparticle pores are developed between calcite, dolomite, quartz, feldspar, clay minerals and pyrite aggregates (Figure 7c). Edges of these pores are generally sharp (Figure 7c). Pores in flaggy and massive rocks are scattered without orientation. Some are triangular due to compaction [52]. Interparticle pores are generally well connected and form a permeable pore network [52–54].

2. Intraparticle pores.

The intraparticle pore is the other important pore type that occurs in the nine lithofacies. The dissolution pores (Figure 7d), intrafossil pores (Figure 7f), intercrystalline pores within pyrite framboids and cleavage-plane pores within clay aggregates are the main intraparticle pore in the study area (Figure 7e,f). The dissolution pores are common in calcite and dolomite, so they are more common in the calcareous lithofacies (LF1, LF4 and LF5)

(Figure 7d). Intercrystalline pores within pyrite framboids (Figure 7e) and cleavage-plane pores within clay aggregates (Figure 7g) commonly occur in LF1, LF2, LF3, LF4 and LF6. There are relatively few organic-matter pores in the study area (Figure 7h).

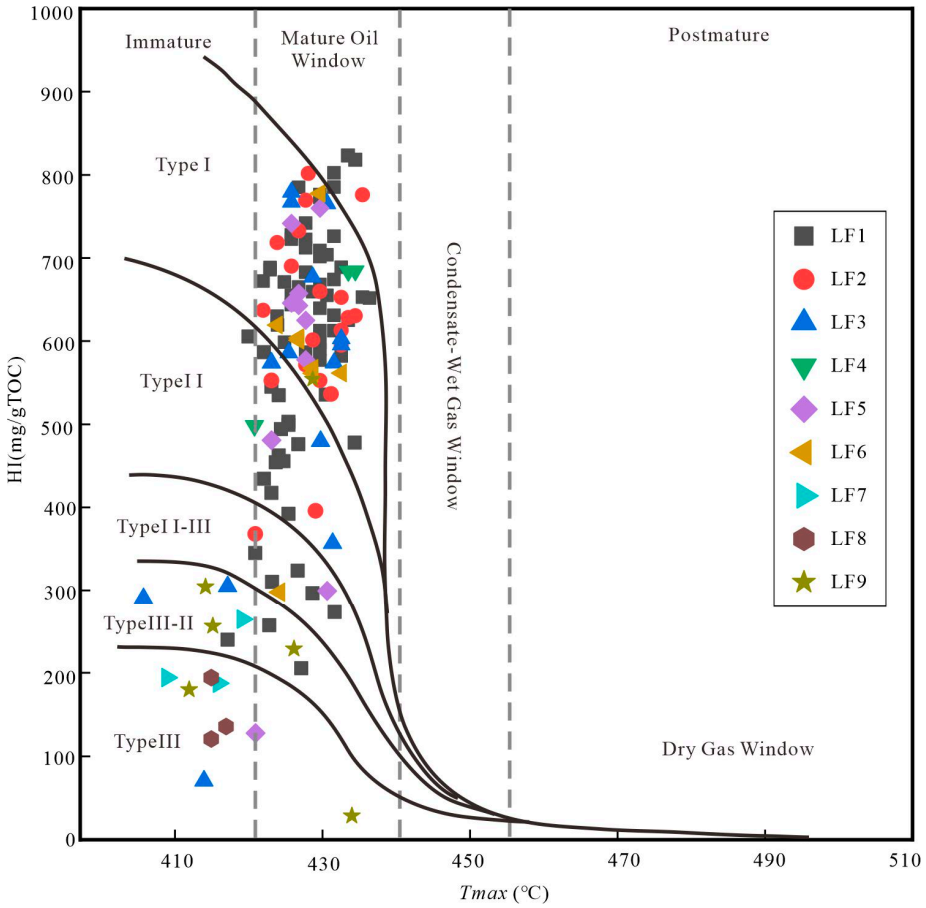

Figure 6. The plot of the hydrogen index (HI) versus the pyrolysis temperature of maximum yield of pyrolysate (T_{max}) for different lithofacies in Es4s in Dongying Depression that displays the kerogen types and the thermal maturity stages (modified from [50]).

3. Lamina fissures.

Lamina fissures are important storage space and flow paths in LF1 and LF2. Lamina fissures occur between the contiguous laminae which are distinguished by different components (Figure 7a). Lamina fissures extend well laterally and their widths vary from 2 μm to 6 μm. They connect the intergranular pores in different laminae.

4. Fractures.

Fractures are also important flow paths in the study object. Structural fractures are well developed in cores. Microfractures can be observed under an optical microscope (Figure 7i) and FESEM. Some are open while some are cemented by calcite. Fractures occur in all nine lithofacies but more commonly in LF1, LF2, LF3, LF4 and LF6 for higher content of brittle mineral. Fractures connect the pores and the laminae fissures.

4.4.2. Pore Size Distribution and Pore Structures Characteristics

Nuclear magnetic resonance is an effective method to reflect the full-scale pore size distribution in the reservoir rocks [55,56]. The plots of the T_2 spectra of the nine lithofacies are shown in Figure 8. It presents three peaks, i.e., p1 at <1 ms, p2 at 10–60 ms and p3 at >100 ms, which, respectively, correspond to micropores, mesopores and macropores. In Figure 8, a distinct high amplitude p1 peak can be seen, while there are small amplitude p2

and p3 peaks. This indicates numerous micropores account for a relatively high proportion in the pore volume and macropores are a minority.

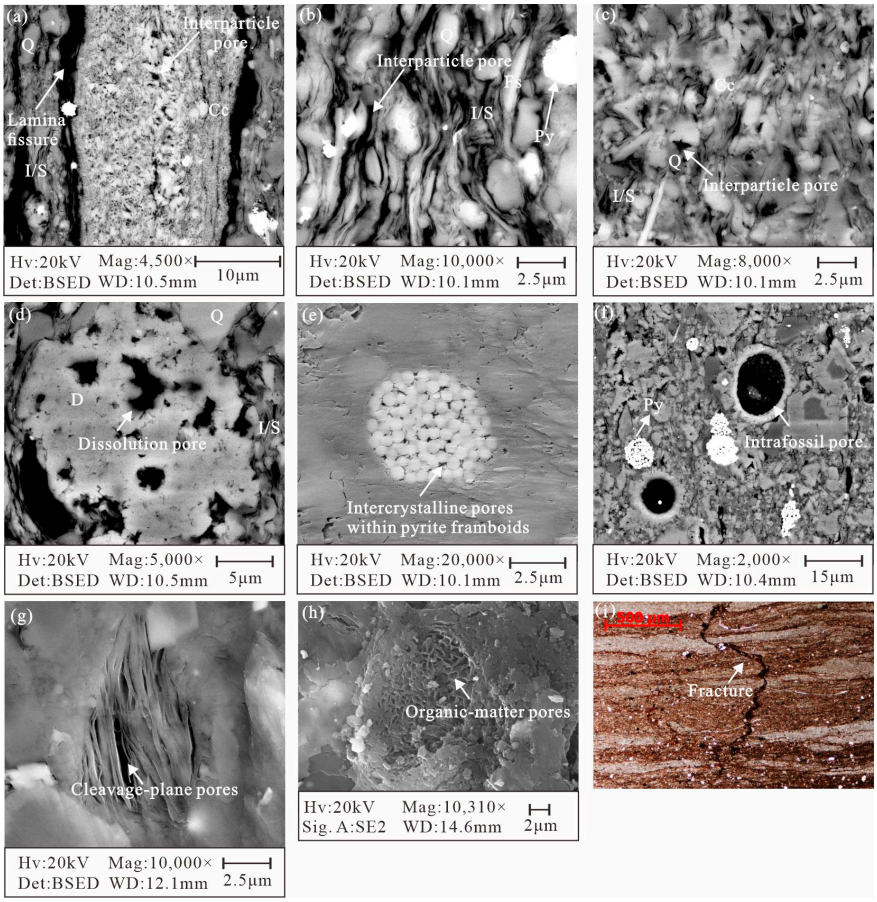

Figure 7. (**a**) Interparticle pores in carbonate laminae. Well GX 27, 2313.75 m. (**b**) Interparticle pores in clay laminae, Well GX27, 2311.53 m. (**c**) Interparticle pores in massive rocks. Well GX27, 2303.18 m. (**d**) Dissolution pores in dolomite. Well GX27, 2317.29 m. (**e**) Intercrystalline pores within pyrite framboids. Well NY1, 3454.4 m. (**f**) Intrafossil pores. Well GX 27, 2300.91 m. (**g**) Cleavage-plane pores within clay grains. Well NX55, 3787.56 m. (**h**) Organic-matter pores. Well N55X1, 3572.98 m. (**i**) Fractures. Well NY1, 3443.55 m.

Nitrogen adsorption is an effective method for studying the micropores [40,57,58]. IUPAC grouped physisorption isotherms into six types and eight subtypes [58]. From Figure 9, the adsorption isotherms of the nine lithofacies can be divided into three stages, which makes them S-shaped, in accordance with Type II [58]. When the relative pressure is low ($P/P_0 < 0.4$), the adsorption amount is low and slowly increases as the relative pressure increases. After that, the adsorption isotherm reaches the middle section, which increases almost linearly as the relative pressure varies from 0.4 to 0.8. At the end of the adsorption isotherm ($0.8 < P/P_0 < 1.0$), the adsorption amount increases sharply as the relative pressure approaches 1. In addition, the hysteresis loop forms between the adsorption isotherm and the desorption isotherm [58,59]. Six characteristic types of hysteresis loops were identified to describe pore morphology [58]. The hysteresis loop of Type H2 is characterized by a very steep desorption isotherm with a sharp inflection point in the middle section. The Type H2 hysteresis loop indicates the ink-bottle-shaped pores are dominant in rocks [58]. It is noted that the hysteresis loops of nine lithofacies present this characteristic. Moreover, the hysteresis loop of Type H3 has the feature that the desorption branch is almost parallel to the adsorption branch in the middle section, resulting in a narrow hysteresis loop [59]. The Type H3 hysteresis loop is given by slit-shaped pores in rocks [58]. The hysteresis loops

of LF3, LF4, LF5, LF6, LF7, LF8 and LF9 exhibit this attribute. Therefore, the hysteresis loops of LF1 and LF2 are Type H2. This indicates that in LF1 and LF2, the ink-bottle-shaped pores are dominant. The hysteresis loops of LF3, LF4, LF5, LF6, LF7, LF8 and LF9 possess characteristics of both Type H2 and Type H3 simultaneously. Consequently, the hysteresis loops of them are Type H2-H3, which indicates that ink-bottle-shaped pores and slit-shaped pores coexist in them [40,58].

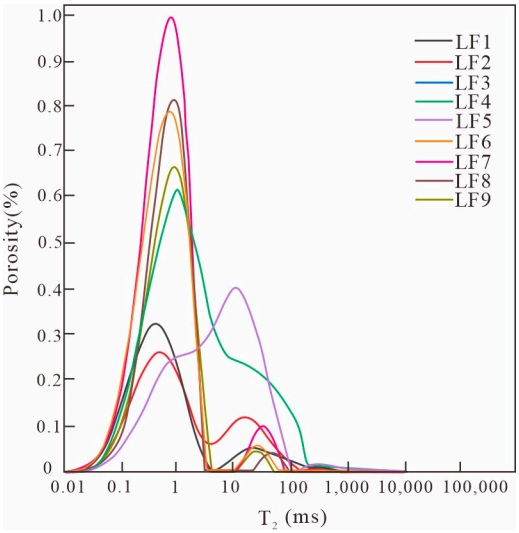

Figure 8. The NMR T_2 spectra of the nine lithofacies in Es4s Dongying Depression.

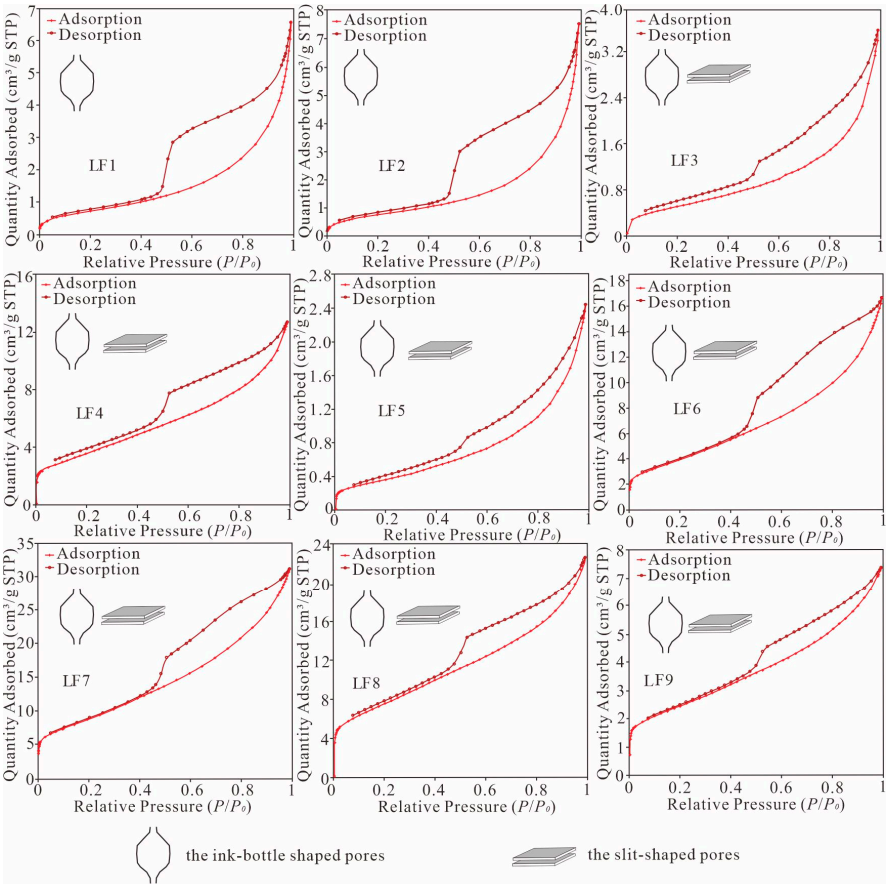

Figure 9. The physisorption isotherms and hysteresis loops of the nine lithofacies in Es4s Dongying Depression.

5. Discussion

5.1. Deposition Processes and Deposition Model

Beddings reflect the way that sediments accumulate, so they are significant sedimentary structures recording the deposition processes [18,60]. As to the fine-grained sedimentary rocks, the deposition processes commonly include pelagic and hemipelagic settling, hemiturbiditic and turbidity currents, contouritic deposition, hyperpycnal flow, debris flow, slides and slumps, chemical processes, biological processes and biochemical processes [21,29,61].

LF1 and LF2 are laminated lithofacies. They are formed by the carbonate lamina and the clay lamina alternating vertically. The rhythmical succession of laminae reveals a cycle of deposition which is commonly driven by seasonal climate variability [62,63]. During the deposition period of the Es4s, the Dongying Depression was located in the mid-latitude site where the climate varied with seasons. In warm seasons, microorganism bloomed and induced the precipitation of carbonate minerals that formed into the light laminae [64,65]. When it turned cold, microorganisms decayed. The terrigenous particles became the dominant sediment supplies [66]. When the paleosalinity in the water during the deposition period is high, it was conducive to the crystallization of carbonate minerals [9,29], thus tending to deposit LF1. In contrast, LF2 occurred. Both LF1 and LF2 are deposited in the deep lake so the type of organic matter in them is Type I and Type II [67].

The unconsolidated sediments can be re-suspended, mixed and redeposited when influenced by gravity, wave and currents [68]. The original laminae were destroyed and the mixed sediments formed flaggy and massive beddings. As a result of these episodic redepositional events, such as turbidity currents, slides and slumps, LF3, LF4 and LF6 occur as interbeds in LF1 and LF2 (Figure 10) [69]. They have similar composition and organic matter to LF1 and LF2, which are deposited from suspension. Bioturbation is another important redeposition which totally changes the original beddings and generally results in massive lithofacies (LF5) [63,68]. Moreover, thick massive dolomitic fine-grained sedimentary rocks are related to the biological processes [21,24]. The types of organic matter in LF5 are Type I and Type II which also indicates they are deposited in the deep lake [67]. In LF7, LF8 and LF9, the organic matter in them is Type III-II and Type III which suggests they are terrigenous [67]. The massive bedding, the high content of terrigenous particles and the organic matter origin reveal that LF7, LF8 and LF9 resulted from strong terrigenous input events (Figure 11) [65,67]. Based on the statistics and analysis, we found that LF1 and LF2 are dominant in the study area.

5.2. Pore Structures

Based on the nuclear magnetic resonance, the pores in the study objects vary from micropores to macropores but micropores are dominant [70]. With the FESEM, it is easy to observe the morphology and distribution of the pores whose diameters are more than 100 nm [40]. These pores include intergranular pores (between carbonate crystals, quartz, feldspar, pyrite framboids and clay aggregates), dissolution pores, lamina fissures and fractures. In the laminated lithofacies (LF1 and LF2), the mineral crystals and particles are arranged in an orderly manner. The intergranular pores between them are polygonal, and the long axes are commonly parallel to the orientation of the lamina. However, due to redeposition, the mineral crystals and particles in flaggy (LF3 and LF4) and massive (LF5, LF6, LF7, LF8 and LF9) lithofacies are disorderly so that the pores are not obviously orientated.

As major pore types, the morphology of micropores in rocks with different beddings are in different shapes. Under the FESEM, the intergranular pores are polygonal and dissolution pores are elliptic [59]. As the carbonate laminae and the clay laminae are distinctly separate, the carbonate crystals in the carbonate laminae and the quartz, feldspar, pyrite framboids and clay aggregates in the clay laminae, respectively, form into polygonal intergranular pores (Figure 7a,b). These polygonal and elliptic pores are regarded as ink-bottle-shaped pores, which is accordance with the analysis of hysteresis loops [40,58,59]. Therefore, micropores in the laminated lithofacies (LF1 and LF2) are ink-bottle-shaped.

However, in the flaggy (LF3 and LF4) and massive (LF5, LF6, LF7, LF8 and LF9) lithofacies, as they resulted from redeposition or event deposition, the mineral crystals and particles are mixed [63]. The carbonate crystals, quartz, feldspar and pyrite framboids are mainly surrounded by the clay minerals so that there is less contact between these rigid minerals and particles. Therefore, the quantity of ink-bottle-shaped intergranular pores between the carbonate crystals, quartz, feldspar and pyrite framboids reduces obviously. Instead, because illites and illite/smectite mixed layers are the main clay minerals in the research object, numerous slit-shaped interparticle pores resulted from the plate-like aggregates of them. Therefore, the hysteresis loops of them present to be Type H2-H3, which indicates the ink-bottle-shaped pores and slit-shaped pores coexist [40,58,59]. Moreover, the higher the content of the clay minerals, the more slit-shaped pores there are. Then, hysteresis loops are closer to Type H3. In addition, fractures are developed in all the nine lithofacies, but are more common in the LF1, LF4, LF5 and LF8 due to the high brittle mineral content.

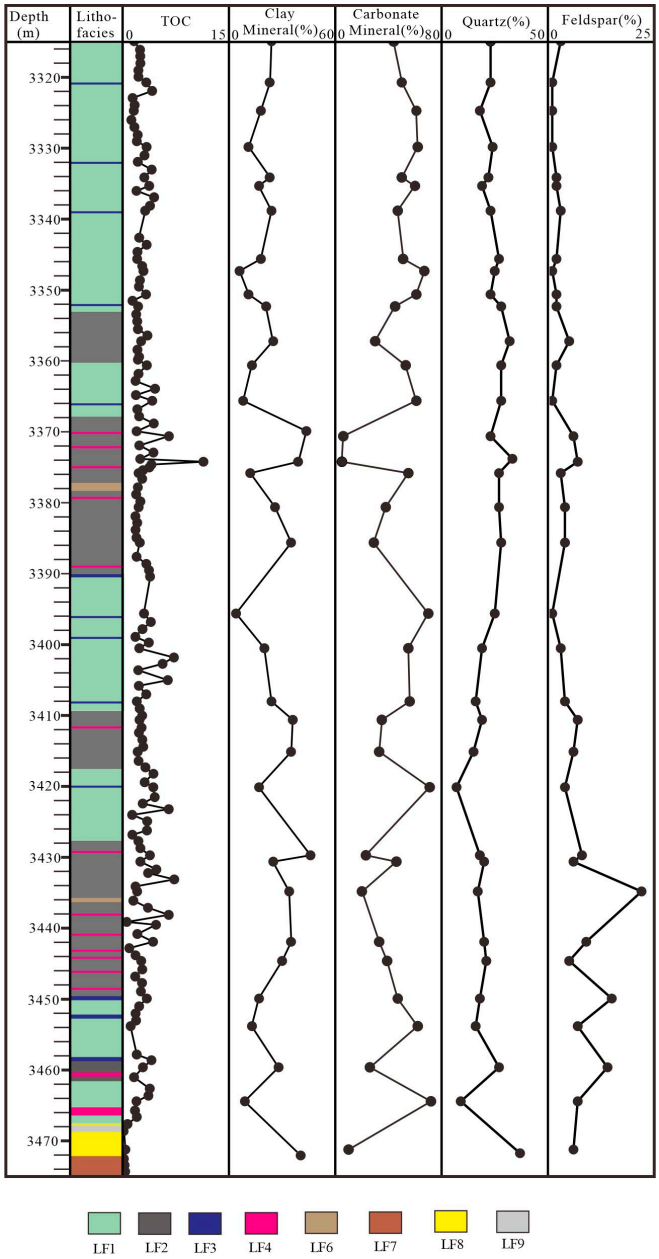

Figure 10. The main mineral composition in different lithofacies of the Es4s shale in well NY1.

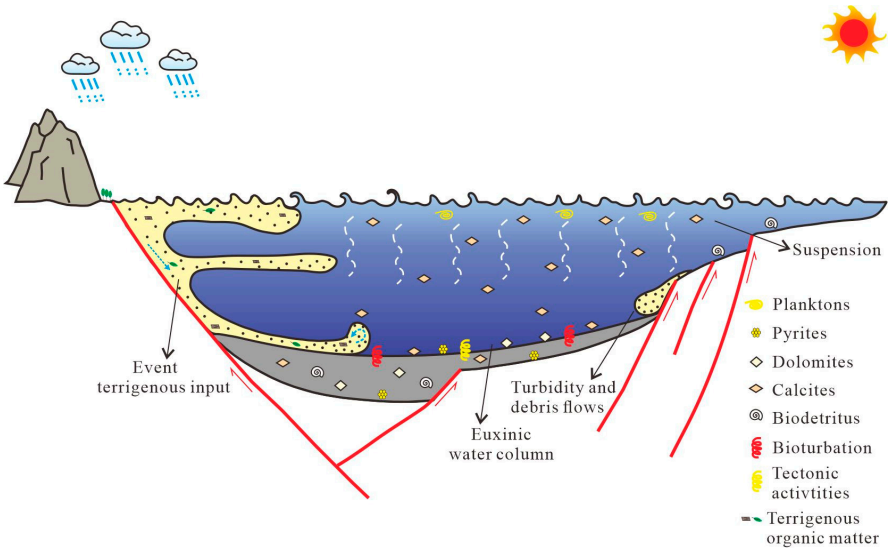

Figure 11. Generalized deposition model showing depositional processes for the fine-grained sedimentary rocks in Es4s in Dongying Depression.

According to the obsevation via FESEM, the intergranular pores are dominant in all the lithofacies and they have better connectivity than the intraparticle pores.

5.3. Controlling Effect of Deposition Processes on Lithofacies and Reservoir Characteristics

Based on the analysis above, the deposition processes determine the composition, the type of organic matter, and the size and arrangement of minerals and particles in the fined-grained sedimentary rocks. The arrangements of minerals and particles determine the beddings and the pore structures. The composition and the beddings are important factors in lithofacies classification. The lithofacies rich in brittle mineral easily crack so fractures commonly occur in them. The dissolution pores are common in the carbonate-rich lithofacies. Therefore, the deposition processes control the lithofacies and reservoir characteristics of the fined-grained sedimentary rocks. The diagenesis also plays an important role in reservoir characteristics, which mainly works after deposition. The deposition processes laid the foundation of the mineral composition and pore structures.

6. Conclusions

Based on mineral composition, the content of organic matter and the beddings, the fine-grained sedimentary rocks in Es4s in Dongying Depression were divided into nine lithofacies: middle-high organic laminated calcareous fine-grained sedimentary rocks (LF1), middle-high organic laminated mixed fine-grained sedimentary rocks (LF2), middle-high organic flaggy mixed fine-grained sedimentary rocks (LF3), middle-high organic flaggy calcareous fine-grained sedimentary rocks (LF4), middle-high organic massive calcareous fine-grained sedimentary rocks (LF5), middle organic massive mixed fine-grained sedimentary rocks (LF6), low organic massive argillaceous fine-grained sedimentary rocks (LF7), low organic massive felsic fine-grained sedimentary rocks (LF8) and low organic massive mixed fine-grained sedimentary rocks (LF9). LF1 and LF2 are deposited from suspension. LF3, LF4, LF5 and LF6 are formed by redeposition. LF7, LF8 and LF9 are affected by terrigenous input events. The pores in the laminated lithofacies are dominated by the ink-bottle-shaped sort. In the flaggy and massive lithofacies, ink-bottle-shaped pores and slit-shaped pores coexist. The storage properties of the ink-bottle-shaped sort are better than the slit-shaped pores so LF1 and LF2 are the best targets for shale oil exploration and LF3, LF4, LF5 and LF6 are the second best. The deposition processes control the lithofacies and reservoir characteristics of the fined-grained sedimentary rocks.

Author Contributions: Conceptualization, Z.J. and Y.Y.; methodology, Y.Y.; software, Y.Y.; formal analysis, Y.Y.; investigation, Y.Y., Z.Z. and C.Y.; writing—original draft preparation, Y.Y.; review Z.J. and J.Z.; funding acquisition, Z.J. All authors have read and agreed to the published version of the manuscript.

Funding: This research was funded by National Major Research Program for Science and Technology of China (Grant No. 2017ZX05009-002) and National Natural Science Foundation of China (Grant No. 41772090).

Data Availability Statement: Data will be made available on request.

Acknowledgments: We sincerely appreciate the help provided by the Geoscience Research Institute of the Shengli Oilfield, SINOPEC, Dongying City, Shandong Province. Also, we want to thank Xin Lei for her help and advice. Last but not least, I would like to express my deepest gratitude to editors and anonymous reviewers for their valuable time, careful work and constructive suggestions which are helpful to improve this paper.

Conflicts of Interest: The authors declare no conflict of interest.

References

1. Slatt, R.M.; O'Brien, N.R. Pore types in the Barnett and Woodford gas shales: Contribution to understanding gas storage and migration pathways in fine-grained rocks. *AAPG Bull.* **2011**, *95*, 2017–2030. [CrossRef]
2. Jarvie, D.M. Shale resource systems for oil and gas: Part 2—Shale-oil resource systems. In *Shale Reservoirs—Giant Resources for the 21st Century: AAPG Memoir*; Breyer, J.A., Ed.; Worldwide Geochemistry, LLC: Humble, TX, USA, 2012; Volume 97, pp. 89–119.
3. Liang, C.; Wu, J.; Cao, Y.; Liu, K.; Khan, D. Storage space development and hydrocarbon occurrence model controlled by lithofacies in the Eocene Jiyang Sub-basin, East China: Significance for shale oil reservoir formation. *J. Pet. Sci. Eng.* **2022**, *215*, 110631. [CrossRef]
4. Loucks, R.G.; Ruppel, S.C. Mississippian Barnett Shale: Lithofacies and depositional setting of a deep-water shale-gas succession in the Fort Worth Basin, Texas. *AAPG Bull.* **2007**, *91*, 579–601. [CrossRef]
5. Jarvie, D.M.; Hill, R.J.; Ruble, T.E.; Pollastro, R.M. Unconventional shale-gas systems: The Mississippian Barnett Shale of north-central Texas as one model for thermogenic shale-gas assessment. *AAPG Bull.* **2007**, *91*, 475–499. [CrossRef]
6. Aplin, A.C.; Macquaker, J.H.S. Mudstone diversity: Origin and implications for source, seal, and reservoir properties in petroleum systems. *AAPG Bull.* **2011**, *95*, 2031–2059. [CrossRef]
7. Schieber, J. Shale microfabrics and pore development: An overview with emphasis on the importance of depositional processes. In *Gas Shale of the Horn River Basin*; Canadian Society of Petroleum Geologists: Calgary, AB, Canada, 2011; pp. 115–119.
8. Zou, C.; Yang, Z.; Cui, J.; Zhu, R.; Hou, L.; Tao, S.; Yuan, X.; Wu, S.; Lin, S.; Wang, L.; et al. Formation mechanism, geological characteristics and development strategy of nonmarine shale oil in China. *Pet. Explor. Dev.* **2013**, *40*, 15–27. [CrossRef]
9. Liang, C.; Wu, J.; Jiang, Z.; Cao, Y.; Song, G. Sedimentary environmental controls on petrology and organic matter accumulation in the upper fourth member of the Shahejie Formation (Paleogene, Dongying Depression, Bohai Bay Basin, China). *Int. J. Coal Geol.* **2018**, *186*, 1–13. [CrossRef]
10. Li, Q.; You, X.; Jiang, Z.; Wu, S.; Zhang, R. Lithofacies and reservoir characterization of a source-controlled carbonate succession in a lacustrine rift basin, the Shulu Sag of Bohai Bay Basin, East China. *J. Pet. Sci. Eng.* **2020**, *192*, 107180. [CrossRef]
11. Hemmesch, N.T.; Harris, N.B.; Mnich, C.A.; Selby, D. A sequence-stratigraphic framework for the Upper Devonian Woodford Shale, Permian Basin, west Texas. *AAPG Bull.* **2014**, *98*, 23–47. [CrossRef]
12. Liang, C.; Jiang, Z.; Yang, Y.; Wei, X. Shale lithofacies and reservoir space of the Wufeng–Longmaxi Formation, Sichuan Basin, China. *Pet. Explor. Dev.* **2012**, *39*, 736–743. [CrossRef]
13. Pan, S.; Zou, C.; Yang, Z.; Dong, D.; Wang, Y.; Wang, S.; Wu, S.; Huang, J.; Liu, Q.; Wang, D.; et al. Methods for shale gas play assessment: A comparison between Silurian Longmaxi shale and Mississippian Barnett shale. *J. Earth Sci.* **2015**, *26*, 285–294. [CrossRef]
14. Li, Y.; Wang, X.; Wu, B.; Li, G.; Wang, D. Sedimentary facies of marine shale gas formations in Southern China: The Lower Silurian Longmaxi Formation in the southern Sichuan Basin. *J. Earth Sci.* **2016**, *27*, 807–822. [CrossRef]
15. Liang, C.; Jiang, Z.; Cao, Y.; Zhang, J.; Guo, L. Sedimentary characteristics and paleoenvironment of shale in the Wufeng-Longmaxi Formation, North Guizhou Province, and its shale gas potential. *J. Earth Sci.* **2017**, *28*, 1020–1031. [CrossRef]
16. Jiang, Z.; Liang, C.; Wu, J.; Zhang, J.; Zhang, W.; Wang, Y.; Liu, H.; Chen, X. Several issues in sedimentological studies on hydrocarbon-bearing fine-grained sedimentary rocks. *Acta Pet. Sin.* **2013**, *34*, 1031–1039. (In Chinese with English Abstract)
17. Burton, D.; Woolf, K.; Sullivan, B. Lacustrine depositional environments in the Green River Formation, Uinta Basin: Expression in outcrop and wireline logs. *AAPG Bull.* **2014**, *98*, 1699–1715. [CrossRef]
18. Lazar, O.R.; Bohacs, K.M.; Macquaker, J.H.S.; Schieber, J.; Demko, T.M. Capturing key attributes of fine-grained sedimentary rocks in outcrops, cores, and thin sections: Nomenclature and description guidelines. *J. Sediment. Res.* **2015**, *85*, 230–246. [CrossRef]
19. Wang, Y.; Liang, C.; Sun, X. Shale oil reservoir characteristics and enrichment in the Jiyang Depression, Bohai Bay Basin, East China. *J. Earth Sci.* **2017**, *28*, 977–986. [CrossRef]

20. Wang, M.; Guo, Z.; Jiao, C.; Lu, S.; Li, J.; Xue, H.; Li, J.; Li, J.; Chen, G. Exploration progress and geochemical features of lacustrine shale oils in China. *J. Pet. Sci. Eng.* **2019**, *178*, 975–986. [CrossRef]
21. Jiang, Z.; Kong, X.; Yang, Y.; Zhang, J.; Zhang, Y.; Wang, L.; Yuan, X. Multi-source genesis of continental carbonate-rich fine-grained sedimentary rocks and hydrocarbon sweet spots. *Pet. Explor. Dev.* **2021**, *48*, 30–42. [CrossRef]
22. Li, Q.; Wu, S.; Xia, D.; You, X.; Zhang, H.; Lu, H. Major and trace element geochemistry of the lacustrine organic-rich shales from the Upper Triassic Chang 7 Member in the southwestern Ordos Basin, China: Implications for paleoenvironment and organic matter accumulation. *Mar. Pet. Geol.* **2020**, *111*, 852–867. [CrossRef]
23. Huang, C.; Zhang, J.; Wang, H.; Jiang, S. Lacustrine shale deposition and variable tectonic accommodation in the rift basins of the Bohai Bay Basin in Eastern China. *J. Earth Sci.* **2015**, *26*, 700–711. [CrossRef]
24. Kong, X. *Sedimentary Characteristics, Origin and Hydrocarbon Accumulation of Lacustrine Carbonate-Bearing Fine-Grained Sedimentary Rocks*; China University of Geosciences (Beijing): Beijing, China, 2020.
25. Ma, Y.; Fan, M.; Lu, Y.; Liu, H.; Hao, Y.; Xie, Z.; Liu, Z.; Li, P.; Du, X.; Hu, H. Climate-driven paleolimnological change controls lacustrine mudstone depositional process and organic matter accumulation: Constraints from lithofacies and geochemical studies. *Int. J. Coal Geol.* **2016**, *167*, 103–118. [CrossRef]
26. Liu, B.; Bechtel, A.; Gross, D.; Fu, X.; Li, X.; Sachsenhofer, R.F. Middle Permian environmental changes and shale oil potential evidenced by high-resolution organic petrology, geochemistry and mineral composition of the sediments in the Santanghu Basin, Northwest China. *Int. J. Coal Geol.* **2018**, *185*, 119–137. [CrossRef]
27. Macquaker, J.H.S.; Bohacs, K.M. On the accumulation of mud. *Science* **2007**, *318*, 1734–1735. [CrossRef]
28. Plint, A.G. Mud dispersal across a Cretaceous prodelta: Storm-generated, wave-enhanced sediment gravity flows inferred from mudstone microtexture and microfacies. *Sedimentology* **2014**, *61*, 609–647. [CrossRef]
29. Liang, C.; Jiang, Z.; Cao, Y.; Wu, J.; Wang, Y.; Hao, F. Sedimentary characteristics and origin of lacustrine organic-rich shales in the salinized Eocene Dongying Depression. *GSA Bull.* **2018**, *130*, 154–174. [CrossRef]
30. Xie, X.; Li, M.; Littke, R.; Huang, Z.; Ma, X.; Jiang, Q.; Snowdon, L.R. Petrographic and geochemical characterization of microfacies in a lacustrine shale oil system in the Dongying Sag, Jiyang Depression, Bohai Bay Basin, Eastern China. *Int. J. Coal Geol.* **2016**, *165*, 49–63. [CrossRef]
31. Zhang, L.; Li, Z.; Zhu, R.; Li, J.; Zhang, L. Resource potential of shale gas in Paleogene in Jiyang Depression. *Nat. Gas Ind.* **2008**, *28*, 26–29. (In Chinese with English Abstract)
32. Zhang, L.; Bao, Y.; Li, J.; Li, Z.; Zhu, R.; Zhang, J. Movability of lacustrine shale oil: A case study of Dongying Sag, Jiyang Depression, Bohai Bay Basin. *Pet. Explor. Dev.* **2014**, *41*, 703–711. [CrossRef]
33. Wu, J.; Jiang, Z.; Qian, K.; Xu, D. Characteristics of salinization mechanism on the upper part of fourth member of Shahejie Formation in the Dongying Sag, Shandong Province. *Acta Geosci. Sin.* **2014**, *35*, 733–740. (In Chinese with English Abstract) [CrossRef]
34. Qiao, R.; Chen, Z.; Li, C.; Wang, D.; Gao, Y.; Zhao, L.; Li, Y.; Liu, J. Geochemistry and accumulation of petroleum in deep lacustrine reservoirs: A case study of Dongying Depression, Bohai Bay Basin. *J. Pet. Sci. Eng.* **2022**, *213*, 110433. [CrossRef]
35. He, J.; Ding, W.; Jiang, Z.; Li, A.; Wang, R.; Sun, Y. Logging identification and characteristic analysis of the lacustrine organic-rich shale lithofacies: A case study from the Es3L shale in the Jiyang Depression, Bohai Bay Basin, Eastern China. *J. Pet. Sci. Eng.* **2016**, *145*, 238–255. [CrossRef]
36. Hu, Q.; Zhang, Y.; Meng, X.; Li, Z.; Xie, Z.; Li, M. Characterization of micro-nano pore networks in shale oil reservoirs of Paleogene Shahejie Formation in Dongying Sag of Bohai Bay Basin, East China. *Pet. Explor. Dev.* **2017**, *44*, 720–730. [CrossRef]
37. Bai, C.; Yu, B.; Han, S.; Shen, Z. Characterization of lithofacies in shale oil reservoirs of a lacustrine basin in eastern China: Implications for oil accumulation. *J. Pet. Sci. Eng.* **2020**, *195*, 107907. [CrossRef]
38. Zhang, J.G.; Jiang, Z.X.; Liang, C.; Wu, J.; Xian, B.Z.; Li, Q. Lacustrine massive mudrock in the Eocene Jiyang Depression, Bohai Bay Basin, China: Nature, origin and significance. *Mar. Pet. Geol.* **2016**, *77*, 1042–1055. [CrossRef]
39. Chen, Z.H.; Wang, T.G.; Liu, Q.; Zhang, S.C.; Zhang, L.Y. Quantitative evaluation of potential organic-matter porosity and hydrocarbon generation and expulsion from mudstone in continental lake basins: A case study of Dongying Sag, Eastern China. *Mar. Pet. Geol.* **2015**, *66*, 906–924. [CrossRef]
40. Zhang, P.; Lu, S.; Li, J. Characterization of pore size distributions of shale oil reservoirs: A case study from Dongying Sag, Bohai Bay Basin, China. *Mar. Pet. Geol.* **2019**, *100*, 297–308. [CrossRef]
41. Wang, H.; Wu, W.; Chen, T.; Yu, J.; Pan, J. Pore structure and fractal analysis of shale oil reservoirs: A case study of the Paleogene Shahejie Formation in the Dongying Depression, Bohai Bay, China. *J. Pet. Sci. Eng.* **2019**, *177*, 711–723. [CrossRef]
42. Zhang, L.; Chen, Z.; Li, Z.; Zhang, S.; Li, J.; Liu, Q.; Zhu, R.; Zhang, J.; Bao, Y. Structural features and genesis of microscopic pores in lacustrine shale in an oil window: A case study of the Dongying Depression. *AAPG Bull.* **2019**, *103*, 1889–1924. [CrossRef]
43. Jiang, Z. *Sedimentary Dynamics of Wind Field-Source-Basin System New Concept for Interpretation and Prediction*; Springer: Singapore, 2018; p. 81.
44. Wu, J.; Jiang, Z. Division and characteristics of shale parasequences in the upper fourth member of the Shahejie Formation, Dongying Depression, Bohai Bay Basin, China. *J. Earth Sci.* **2017**, *28*, 1006–1019. [CrossRef]
45. Liang, C.; Cao, Y.; Jiang, Z.; Wu, J.; Guoqi, S.; Wang, Y. Shale oil potential of lacustrine black shale in the Eocene Dongying depression: Implications for geochemistry and reservoir characteristics. *AAPG Bull.* **2017**, *101*, 1835–1858. [CrossRef]

46. Guo, X.W.; Liu, K.Y.; He, S.; Song, G.Q.; Wang, Y.S.; Hao, X.F.; Wang, B.J. Petroleum generation and charge history of the northern Dongying Depression, Bohai Bay Basin, China: Insight from integrated fluid inclusion analysis and basin modelling. *Mar. Pet. Geol.* **2012**, *32*, 21–35. [CrossRef]
47. Jiang, Z.; Duan, H.; Liang, C.; Wu, J.; Zhang, W.; Zhang, J. Classification of hydrocarbon-bearing fine-grained sedimentary rocks. *J. Earth Sci.* **2017**, *28*, 693–976. [CrossRef]
48. Spears, D.A. Towards a classification of shales. *J. Geol. Soc. Lond.* **1980**, *137*, 125–129. [CrossRef]
49. Luan, G.; Dong, C.; Azmy, K.; Lin, C.; Ma, C.; Ren, L.; Zhu, Z. Origin of bedding-parallel fibrous calcite veins in lacustrine black shale: A case study from Dongying Depression, Bohai Bay Basin. *Mar. Pet. Geol.* **2019**, *102*, 873–885. [CrossRef]
50. Mukhopadhyay, P.K.; Wade, J.A.; Kruge, M.A. Organic facies and maturation of Jurassic/Cretaceous rocks, and possible oil-source rock correlation based on pyrolysis of asphaltenes, Scotian Basin, Canada. *Org. Geochem.* **1995**, *22*, 85–104. [CrossRef]
51. Kong, X.; Jiang, Z.; Han, C.; Zheng, L.; Zhang, J. The tight oil of lacustrine carbonate-rich rocks in the Eocene Shulu Sag: Implications for lithofacies and reservoir characteristics. *J. Pet. Sci. Eng.* **2019**, *175*, 547–559. [CrossRef]
52. Loucks, R.G.; Reed, R.M.; Ruppel, S.C.; Hammes, U. Spectrum of pore types and networks in mudrocks and a descriptive classification for matrix-related mudrock pores. *AAPG Bull.* **2012**, *96*, 1071–1098. [CrossRef]
53. Velde, B. Compaction trends of clay-rich deep sea sediments. *Mar. Geol.* **1996**, *133*, 193–201. [CrossRef]
54. Milliken, K.L.; Reed, R.M. Multiple causes of diagenetic fabric anisotropy in weakly consolidated mud, Nankai accretionary prism, IODP Expedition 316. *J. Struct. Geol.* **2010**, *32*, 1887–1898. [CrossRef]
55. Erik, R.; Singer, P.M.; Tianmin, J.; Rick, L. NMR T_2 distributions in the Eagle Ford Shale: Reflections on pore size. In Proceedings of the SPE Unconventional Resources Conference, The Woodlands, TX, USA, 10–12 April 2013; 2013.
56. Zhang, P.F.; Lu, S.F.; Li, J.G.; Chen, C.; Xue, H.T.; Zhang, J. Petrophysical characterization of oil-bearing shales by low-field nuclear magnetic resonance (NMR). *Mar. Pet. Geol.* **2018**, *89*, 775–785. [CrossRef]
57. Sing, K.S.W.; Everett, D.H.; Haul, R.A.W.; Moscou, L.; Pierotti, R.A.; Rouquérrol, J.; Siemieniewska, T. Reporting physisorption data for gas/solid systems with special reference to the determination of surface area and porosity (Provisional). *Pure Appl. Chem.* **2015**, *5*, 2202–2218. [CrossRef]
58. Thommes, M.; Kaneko, K.; Neimark, A.V.; Olivier, J.P.; Rodriguez-Reinoso, F.; Rouquerol, J.; Sing, K.S.W. Physisorption of gases, with special reference to the evaluation of surface area and pore size distribution (IUPAC Technical Report). *Pure Appl. Chem.* **2015**, *87*, 1051–1069. [CrossRef]
59. Zhang, P.; Lu, S.; Zeng, Z.; Chang, X.; Li, J.; Chen, G.; Zhang, J.; Lin, Z.; Li, J.; Tian, S. Pore structure and fractal character of lacustrine oil-bearing shale from the Dongying Sag, Bohai Bay Basin, China. *Geofluids* **2021**, *2021*, 9945494. [CrossRef]
60. Tucker, M.E. *Sedimentary Petrology an Introduction to the Origin of Sedimentary Rocks*, 3rd ed.; Blackwell Science: Oxford, UK, 2001.
61. Stow, D.A.V.; Huc, A.Y.; Bertrand, P. Depositional processes of black shales in deep water. *Mar. Pet. Geol.* **2001**, *18*, 491–498. [CrossRef]
62. Glenn, C.R.; Kelts, K. Sedimentary rhythms in lake deposits. In *Cycles and Events in Stratigraphy*, 1st ed.; Einsele, G., Ricken, W., Seilacher, A., Eds.; Springer: Berlin/Heidelberg, Germany, 1991; pp. 188–221.
63. Zolitschka, B.; Francus, P.; Ojala, A.E.K.; Schimmelmann, A. Varves in lake sediments—A review. *Quat. Sci. Rev.* **2015**, *117*, 1–41. [CrossRef]
64. Valero-Garces, B.; Morellon, M.; Moreno, A.; Corella, J.P.; Martin-Puertas, C.; Barreiro, F.; Perez, A.; Giralt, S.; Mata-Campo, M.P. Lacustrine carbonates of Iberian Karst Lakes: Sources, processes and depositional environments. *Sediment. Geol.* **2014**, *299*, 1–29. [CrossRef]
65. Kong, X.; Jiang, Z.; Han, C.; Zheng, L.; Zhang, Y.; Zhang, R.; Tian, J. Genesis and implications of the composition and sedimentary structure of fine-grained carbonate rocks in the Shulu Sag. *J. Earth Sci.* **2017**, *28*, 1047–1063. [CrossRef]
66. Zolitschka, B. Varved lake sediments. In *Encyclopedia of Quaternary Science*; Saraswat, R., Nigam, R., Eds.; Elsevier: Amsterdam, The Netherlands, 2007; pp. 3105–3114.
67. Carroll, A.R.; Bohacs, K.M. Lake-type controls on petroleum source rock potential in nonmarine basins. *AAPG Bull.* **2001**, *85*, 1033–1053.
68. Larsen, C.P.S.; MacDonald, G.M. Lake morphometry, sediment mixing and the selection of sites for fine resolution palaeoecological studies. *Quat. Sci. Rev.* **1993**, *12*, 781–792. [CrossRef]
69. Stanley, D.J. Mud redeposition and problems of assessing microfossil, isotopic and radiocarbon data in the Mediterranean. *Mar. Geol.* **1985**, *62*, 381–389. [CrossRef]
70. Yao, Y.; Liu, D.; Che, Y.; Tang, D.; Tang, S.; Huang, W. Petrophysical characterization of coals by low-field nuclear magnetic resonance (NMR). *Fuel* **2010**, *89*, 1371–1380. [CrossRef]